Chemical potential perturbation: A method to predict chemical potentials in periodic molecular simulations

Stan G. Moore and Dean R. Wheeler[a)]
Department of Chemical Engineering, Brigham Young University, 350 CB, Provo, Utah 84602, USA

(Received 27 October 2010; accepted 12 February 2011; published online 17 March 2011)

A new method, called chemical potential perturbation (CPP), has been developed to predict the chemical potential as a function of density in periodic molecular simulations. The CPP method applies a spatially varying external force field to the simulation, causing the density to depend upon position in the simulation cell. Following equilibration the homogeneous (uniform or bulk) chemical potential as a function of density can be determined relative to some reference state after correcting for the effects of the inhomogeneity of the system. We compare three different methods of approximating this correction. The first method uses the van der Waals density gradient theory to approximate the inhomogeneous Helmholtz free energy density. The second method uses the local pressure tensor to approximate the homogeneous pressure. The third method uses the Triezenberg–Zwanzig definition of surface tension to approximate the inhomogeneous free energy density. If desired, the homogeneous pressure and Helmholtz free energy can also be predicted by the new method, as well as binodal and spinodal densities of a two-phase fluid region. The CPP method is tested using a Lennard-Jones (LJ) fluid at vapor, liquid, two-phase, and supercritical conditions. Satisfactory agreement is found between the CPP method and an LJ equation of state. The efficiency of the CPP method is compared to that for Widom's method under the tested conditions. In particular, the new method works well for dense fluids where Widom's method starts to fail. © *2011 American Institute of Physics*. [doi:10.1063/1.3561865]

I. INTRODUCTION

The chemical potential can be related to many different phenomena[1,2] such as phase equilibria, including solubility and osmosis, transport processes such as diffusion, as well as chemical reaction rates. These phenomena are important in the design of many industrial processes. Methods to predict the chemical potential, such as statistical mechanical computations, are particularly useful when experimental data are difficult to obtain.

There are multiple ways to get chemical potentials and other free-energy-related properties from statistical mechanical computations. For instance, one can use thermodynamic integration, Widom's method, and free-energy perturbation methods in general.[3] However, some of these methods such as Widom's may become increasingly inefficient or even fail as the density of the simulation is increased.[3,4]

Widom proposed a simple and elegant method to calculate the chemical potential.[3,5–7] For homogeneous, pure-component NVT systems,

$$\mu^{\text{ex}} = -k_{\text{B}}\,T\,\ln\left\langle \exp\left(-\frac{\triangle U}{k_{\text{B}}\,T}\right)\right\rangle, \tag{1}$$

where μ^{ex} is the chemical potential in excess of an ideal gas, T is the system temperature, k_{B} is Boltzmann's constant, $\triangle U$ is the hypothetical energy of insertion of a test-particle, and $\langle \ldots \rangle$ denotes the canonical average. Widom's method becomes less efficient for dense systems because the probability of a favorable test-particle insertion (little or no overlap with neighboring particles) is low. Related to Widom's method is Bennett's (or the overlapping distribution) method, which uses both hypothetical insertions and deletions to calculate μ^{ex}.[3,8] Several methods have been proposed to increase the efficiency of Widom's and Bennett's methods for dense systems.[9–13]

Other methods also seek to overcome the limitations of Widom's method, including staged-insertion,[14] umbrella sampling,[13,15] expanded ensembles,[16,17] thermodynamic integration,[3] and histogram-distribution methods.[18] These methods can be much more efficient and accurate than Widom's method, but may likewise become less computationally efficient with structured molecules or as the density of the system is increased. For a review of these methods see Ref. 19.

Two Monte Carlo (MC) methods are particularly related to this work. Grand canonical Monte Carlo (GCMC) (Ref. 3) imposes constant chemical potential, temperature, and volume on the system and measures the resulting composition. The chemical potential of an ideal gas reservoir, which can be calculated analytically, is set, and the simulation cell is equilibrated with the reservoir by changing the number of molecules in the simulation cell. After equilibration, the chemical potential of the simulation cell is equal to the known chemical potential of the reservoir.

Gibbs ensemble Monte Carlo (GEMC) (Refs. 3, 20, and 21) uses two simulation cells to equilibrate two phases. The temperature, volume, and total number of molecules of the system remain fixed, but molecules and volume are exchanged between the two simulation cells. After equilibration,

a)Electronic mail: dean_wheeler@byu.edu.

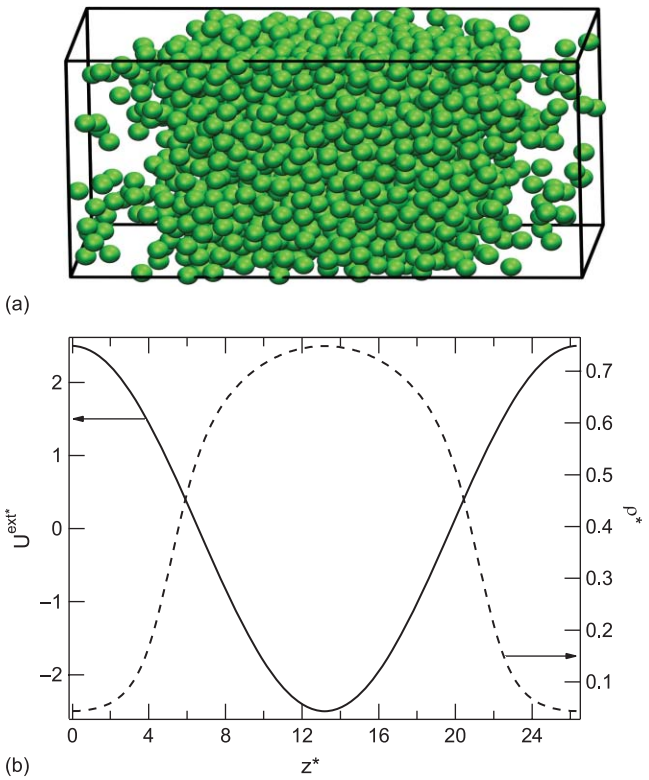

FIG. 1. (a) Snapshot of CPP simulation 1. (b) $U^{\text{ext}}(z)$ and $\rho(z)$ vs position z.

the chemical potentials of the two cells are equal. For pure-component fluids, each cell contains either the liquid or vapor phase, and the coexisting densities of the fluid can be determined. GEMC avoids the formation of an interface between the two phases. Like all MC methods, GCMC and GEMC rely on particle insertions and deletions and become increasingly inefficient as the density of the system increases.

One can also directly simulate phase equilibria using molecular simulations. Unlike GEMC simulations, an interfacial region may form between different phases. This allows the prediction of interfacial properties such as surface tension. (For a review of methods used to obtain surface tension in molecular simulations, see Ref. 22.) However, the presence of an interface may also increase computational cost if this is not the region of interest.[3] The simulation cell is usually elongated in one direction to form a stable interface.[23] Due to the presence of density gradients, standard long-range corrections and cut-offs may no longer be adequate.[22]

Another alternative to insertion-based methods is osmotic molecular dynamics (OMD), developed by Rowley and co-workers.[24,25] OMD uses a semipermeable membrane to achieve chemical equilibrium between two compartments on either side of the membrane. For pure-component systems, the respective compartments contain the fluid at the desired density and the same fluid at a very low density to serve as an ideal gas reference. For liquid mixtures, the respective compartments contain the mixture at the desired composition and the pure liquid as a reference. Tagged molecules are allowed to pass freely through the membrane, while others are completely restricted to one side by a soft-wall external potential until equilibrium is achieved. Homogeneous properties are obtained by excluding inhomogeneous portions of the simulation close to the membrane region.

Powles *et al.* also used a molecular dynamic (MD) simulation with an external potential to create a low-density fluid pocket surrounded by a high-density fluid region.[26] The chemical potential was then measured in the low-density region using Widom's method, allowing one to predict the chemical potential of the high-density region after removing the effects of the external field.[7] No correction due to the inhomogeneity of the system was necessary because the high-density region was virtually homogeneous.

The chemical potential perturbation (CPP) method proposed here can be thought of as a generalization of OMD and the method of Powles *et al.* The CPP method uses a finite external potential which varies periodically in one direction, matching the periodic boundary conditions of the simulation cell. Under the action of this field, the density similarly varies throughout the cell in a periodic fashion. For example, Fig. 1 shows a snapshot of CPP simulation 1 (described below), produced using the VMD software program.[27] Figure 1 also shows the external potential $U^{\text{ext}}(z)$ and resulting density profile $\rho(z)$ of this simulation versus position z.

The CPP method is also related to GCMC and GEMC. Molecules in each differential slice of the CPP simulation are exchanged between neighboring slices, similar to a GEMC simulation. In GCMC, the chemical potential of the system is fixed and the density of the simulation cell is measured after equilibration. In CPP, the external potential is fixed and the density at each location z is then measured after equilibration. We implemented CPP within MD simulations, although it could be used in MC simulations as well. MD simulations avoid particle insertions and more readily allow one to simulate very dense phases.

When one performs an inhomogeneous molecular simulation, it is normally with the intention to obtain phase equilibria properties such as coexisting liquid–vapor densities or interfacial properties such as surface tension. In contrast, with CPP a single inhomogeneous simulation is used to obtain homogeneous (uniform or bulk) properties for the whole range of densities found in the inhomogeneous simulation.

Below, we develop the CPP method for pure-component systems and explain how to correct for effects on the chemical potential due to the inhomogeneity of the fluid. We show results for the Lennard-Jones fluid at vapor, liquid, two-phase, and supercritical conditions.

II. DEVELOPMENT OF THE CPP METHOD

We desire to obtain the chemical potential of a homogeneous fluid corresponding to each density found in an NVT simulation of an inhomogeneous fluid. A simulated fluid may be inhomogeneous due to spontaneous phase splitting, or may be inhomogeneous due to the effects of an external potential acting on the system, or both. In any case, it is necessary to correct for the effects resulting from the inhomogeneity of the system to obtain homogeneous properties.

According to concepts found in density functional theory,[28] one can divide the properties of inhomogeneous fluids into both local and nonlocal terms. Local, or

homogeneous, terms depend only on the condition of the fluid at position **r** in the simulation cell. Because molecules interact over a finite distance, however, the condition at one location affects that of other locations. Nonlocal, or inhomogeneous, terms capture this effect and depend upon the condition of the fluid in the vicinity of position **r**. For example, surface tension is a manifestation of nonlocal effects. We describe below how to obtain homogeneous properties using three different methods.

A. Van der Waals density gradient theory

Van der Waals (VdW) developed a density gradient theory that can be used to predict the surface tension and density profile of an inhomogeneous fluid if the density profile is sufficiently slowly varying.[29–31] Van der Waals proposed that the local free energy density consists of two terms: the homogeneous free energy density and the inhomogeneous free energy density, which depends on the density gradient squared. This theory was later rediscovered by Cahn and Hilliard,[32] and Yang *et al.* obtained a similar result from a rigorous expansion in powers of density derivatives.[33]

Using density gradient theory, an analytical equation of state can be used to predict the surface tension and density profile of an inhomogeneous fluid.[30,34] In other words, information about a homogeneous system is used to predict inhomogeneous or interfacial properties. In the CPP method, the reverse is used: the density profile and other information pertaining to a simulated inhomogeneous system is used to obtain homogeneous properties.

We follow the work of Yang *et al.* and define the total Helmholtz free energy F^{tot} of the system as the volume integral of the Helmholtz free energy density $\psi^{\text{tot}}(\mathbf{r})$, or

$$F^{\text{tot}} = \int \psi^{\text{tot}}(\mathbf{r})\, d\mathbf{r}. \tag{2}$$

For an inhomogeneous system with an external potential $U^{\text{ext}}(\mathbf{r})$, the free energy density can be partitioned into multiple contributions:

$$\psi^{\text{tot}}(\mathbf{r}) = U^{\text{ext}}(\mathbf{r})\,\rho(\mathbf{r}) + \psi^{0}(\mathbf{r}) + \psi^{\text{IH}}(\mathbf{r}), \tag{3}$$

where ρ is the molecular number density. ψ^0 is the free energy density of a homogeneous fluid with temperature and density the same as the inhomogeneous fluid at position **r** and is a local term. ψ^{IH} is the excess free energy density due to the inhomogeneity of the system and is a nonlocal term. Throughout this work, we assume the density varies only in the z direction. Equation (3) then becomes

$$\psi^{\text{tot}}(z) = U^{\text{ext}}(z)\,\rho(z) + \psi^{0}(z) + \psi^{\text{IH}}(z). \tag{4}$$

Yang *et al.* rigorously showed that a density gradient term can be used to approximate $\psi^{\text{IH}}(z)$ as

$$\psi^{\text{IH}}(z) = \frac{1}{2}c(\rho)\,\rho'(z)^2 + \mathcal{O}(\nabla^4\rho), \tag{5}$$

where $\rho'(z) = d\rho/dz$ and $c(\rho)$ is called the influence parameter and is given as

$$c(\rho) = \frac{2}{3}\pi\, k_{\text{B}}\, T \int dr_{12}\, r_{12}^4\, C^0(r_{12}, \rho), \tag{6}$$

where r_{12} is the molecular pair-wise distance and $C^0(r_{12}, \rho)$ is the direct correlation function of a homogeneous fluid. The influence parameter c may be also taken to be an empirical constant (independent of temperature and density),[34] as is the case in this work unless otherwise noted. In Eq. (5), the notation $\mathcal{O}(\nabla^4\rho)$ refers to the order of the truncation error, meaning that the neglected terms are proportional to products of density derivatives whose orders sum to 4 or greater. We include this term as a reminder that higher order terms have been neglected in gradient theory.

Equations (3) and (4) do not necessarily describe a system at equilibrium. If we assume equilibrium, then F^{tot} will be minimized subject to the constraints of constant volume V and a fixed number of molecules N. One can use the solution to the Euler-Lagrange equation to minimize F^{tot} with these constraints.[33] This leads to

$$\mu^{\text{tot}} = U^{\text{ext}}(z) + \mu^{0}(z) + \mu^{\text{IH}}(z), \tag{7}$$

where μ^{tot} is the total chemical potential, which is constant at all locations inside the simulation cell, μ^0 is the homogeneous chemical potential, and μ^{IH} is the inhomogeneous chemical potential. The intrinsic chemical potential μ^{int} is defined as $\mu^{\text{int}}(z) = \mu^0(z) + \mu^{\text{IH}}(z)$. We note that Widom's method when applied to an inhomogeneous system gives μ^{int}, not μ^0.[7,31]

Using the Euler–Lagrange equation and the approximation for ψ^{IH} given in Eqs. (5) and (6) gives[33]

$$\mu^{\text{IH}}(z) = -\frac{1}{2}\frac{\partial c(\rho)}{\partial \rho}\,\rho'(z)^2 - c(\rho)\,\rho''(z) + \mathcal{O}(\nabla^4\rho), \tag{8}$$

where $\rho''(z) = d^2\rho/dz^2$.

Rearranging Eq. (7) yields

$$\mu^{0}(z) = -U^{\text{ext}}(z) - \mu^{\text{IH}}(z) + \mu^{\text{tot}}. \tag{9}$$

In the CPP method, U^{ext} is fixed. In this work, the combination of Eqs. (8) and (9) with c taken to be an empirical constant constitute the *VdW method*. Using this method, $\mu^0(z)$ can be determined to within a constant, μ^{tot}, discussed below.

For pure-component systems at constant temperature,[31]

$$\psi^{0}(\rho) = \int \mu^{0}(\rho)\, d\rho - P^*, \tag{10}$$

where P^* is a constant of integration. In the absence of an external field, P^* is equal to the hydrostatic pressure of the system. If desired, the homogeneous Helmholtz free energy density at equilibrium ψ^0 can be obtained from the VdW method by multiplying Eq. (9) by $d\rho/dz$ according to Eq. (10) and integrating with respect to z:

$$\psi^{0}(z) = -\int U^{\text{ext}}(z)\frac{d\rho(z)}{dz}dz + \psi^{\text{IH}}(z) + \mu^{\text{tot}}\,\rho(z) - P^* + \mathcal{O}(\nabla^4\rho), \tag{11}$$

where we have used Eqs. (5) and (8) as well. From the relationship between Gibbs and Helmholtz free energies, the

homogeneous pressure P^0 of a pure-component fluid can be defined as

$$P^0(z) = \mu^0(z)\,\rho(z) - \psi^0(z). \tag{12}$$

The system constants μ^{tot} and P^* can be determined in two ways. First, if the density is low enough at some position in the CPP simulation, they can be determined from the ideal gas chemical potential and pressure. Otherwise, an additional homogeneous simulation using Widom's method or an equation of state (EOS) can be used to determine the chemical potential and pressure at one density found in the CPP simulation. Alternatively, one could determine μ^{tot} by performing Widom insertions at one location in the CPP simulation (generally the planar slice with the lowest density).

B. Pressure tensor

In this section, we describe how to calculate the inhomogeneous pressure tensor $\mathbf{P}(z)$ and show how to approximate corresponding homogeneous properties.

1. Calculation of the pressure tensor

The virial equation can be used to obtain the pressure tensor. Assuming thermal equilibrium, for our system $\mathbf{P}(z)$ can be expressed as[35]

$$\mathbf{P}(z) = k_{\text{B}}\,T\,\rho(z)\,\mathbf{I} + \frac{1}{V}\sum_i \sum_{j<i} \mathbf{f}_{ijn}\,(\mathbf{r}_{ijn})^{\text{T}}\tau_{ijn}(z), \tag{13}$$

where $\mathbf{I}$ is the identity matrix, the notation ijn means that the nearest-image convention is used in conjunction with periodic boundary conditions between molecules i and j, $\mathbf{r}_{ijn}$ is the molecular pair-wise distance, and $\mathbf{f}_{ijn}$ is the intermolecular force. The superscript T refers to the matrix transpose, in this case turning a column vector into a row vector. The double sum is over all unique molecular pairs in the system employing a spherical cut-off based on distance $\mathbf{r}_{ijn}$.

$\tau_{ijn}(z)$ is the contour function that controls how the pressure is distributed spatially with respect to each interacting pair of molecules. The pressure tensor has a well known ambiguity on this issue. There are an infinite number of ways to define the contour,[36] but the contours given by Irving and Kirkwood (IK) (Ref. 35) and Harasima[37] (see also Ref. 38), are most commonly used. We use the IK contour in this paper, which distributes the pressure uniformly along a straight line connecting the interacting pair of molecules (in the nearest-image sense). There are multiple ways to express this mathematically.[39,40] We use

$$\tau_{ijn}(z) = \frac{L_z}{z_{ijn}}[\Theta(z - z_i) - \Theta(z - z_j)] + \frac{\Delta_{ij}}{z_{ijn}}, \tag{14}$$

where Θ is the Heaviside step function, L_z is the length in the z direction, $\Delta_{ij} = -L_z\,\text{trunc}\,[2(z_j - z_i)/L_z]$, $z_{ijn} = z_j - z_i + \Delta_{ij}$, and trunc(x) is the truncation function that removes the fractional part of x and returns the integer part. In practice, $\mathbf{P}(z)$ is calculated with the IK contour using a finite number of slabs normal to the z direction. The N_{s} slabs that contain any part of the line connecting the two molecular centers of mass are determined, and each of these slabs is given $1/N_{\text{s}}$ of the total contribution of pressure from a given pair interaction.[41]

For our system, there are two independent components of the pressure tensor: one normal to the interface, $P_{\text{N}}(z) = P_{zz}(z)$, and one tangential to the interface, $P_{\text{T}}(z) = P_{xx}(z) = P_{yy}(z)$.

2. Restrictions on the normal pressure

For a fluid at equilibrium, mechanical stability introduces a restriction on the normal pressure. In the case of our system,

$$\frac{dP_{\text{N}}(z)}{dz} = \rho(z)\,f^{\text{ext}}(z), \tag{15}$$

where $f^{\text{ext}}(z) = -dU^{\text{ext}}(z)/dz$ is the external force acting on the particles in the system.[31]

Equation (15) can be integrated to obtain

$$P_{\text{N}}(z) = \int \rho(z)\,f^{\text{ext}}(z)\,dz + P^*. \tag{16}$$

For a system at equilibrium, ψ^0 is given by Eq. (11). We can eliminate the integral in Eq. (11) using integration by parts with the help of Eq. (16), giving

$$\psi^0(z) = -U^{\text{ext}}(z)\,\rho(z) - P_{\text{N}}(z) + \psi^{\text{IH}}(z) + \mu^{\text{tot}}\,\rho(z) + \mathcal{O}(\nabla^4\rho). \tag{17}$$

Combining Eqs. (9), (12) and (17) and rearranging yields

$$P_{\text{N}}(z) = P^0(z) + \psi^{\text{IH}}(z) + \mu^{\text{IH}}(z)\,\rho(z) + \mathcal{O}(\nabla^4\rho). \tag{18}$$

Like Eq. (15), Eq. (18) can also be used to verify that the system is at mechanical equilibrium.

3. Obtaining homogeneous properties

For the IK definition of pressure tensor, a Taylor series expansion in density gradients predicts that

$$P_{\text{N}}(z) = P^0(z) + k\left[\frac{1}{2}\rho'(z)^2 - \rho''(z)\,\rho(z)\right] + \mathcal{O}(\nabla^4\rho), \tag{19}$$

and

$$P_{\text{T}}(z) = P^0(z) + \frac{1}{3}k\left[\frac{1}{2}\rho'(z)^2 - \rho''(z)\,\rho(z)\right] + \mathcal{O}(\nabla^4\rho), \tag{20}$$

where k is a constant that depends on the intermolecular potential and radial distribution function of the fluid.[28] (See also Refs. 42 and 43.) In fact, k can be calculated from c [Eq. (6)] used in VdW gradient theory with the use of certain approximations.[28]

If $U^{\text{ext}}(z) = 0$, then P_{N} is constant at all locations in the system, even if there are two phases and an interface present, as shown by Eq. (15). The chemical potential μ^{int} given by Widom's method is also constant in the absence of an external field as shown by Eq. (7). However, if two phases are present,

P_T, P^0, and μ^0 may vary throughout the interface, and P^0 and μ^0 will furthermore exhibit a van der Waals loop.

Combining Eqs. (19) and (20) and solving for P^0 yields

$$P^0(z) = \frac{3}{2}P_T(z) - \frac{1}{2}P_N(z) + \mathcal{O}(\nabla^4\rho). \tag{21}$$

It is not necessary to determine the constant P^* if the IK expressions for pressure [Eqs. (13) and (14)] are used.

Once we have determined P^0, we can obtain μ^0 using the definition of Gibbs free energy (at constant temperature):

$$\mu^0(z) = \int \frac{dP^0(z)}{dz}\frac{1}{\rho(z)}dz + \mu^{tot}. \tag{22}$$

In this paper, we refer to the use of Eqs. (21) and (22) as the *pressure tensor method* of obtaining μ^0. If desired, the free energy density can be obtained from the pressure tensor method by rearranging Eq. (12).

C. TZ method

Here, we show a third method to obtain homogeneous properties using a relation between the surface tension γ and ψ^{IH}. Working equations for surface tension often include a factor of 1/2 to account for the fact that two interfaces are formed in periodic molecular simulations. However, for simplicity, the equations in this section assume a single interface. For a nonperiodic system, the integrals over system length range between $\pm\infty$, and for a periodic system, they range between 0 and L_z.

1. Surface tension

The surface tension is related to the pressure tensor according to[35]

$$\gamma = \int [P_N(z) - P_T(z)]\,dz. \tag{23}$$

The total grand potential Ω^{tot} can be defined as

$$\Omega^{tot} = A\int [\psi^{tot}(z) - \mu^{tot}\,\rho(z)]dz. \tag{24}$$

Ω^{tot} is also related to P_T as[44,45]

$$\Omega^{tot} = -A\int P_T(z)dz. \tag{25}$$

Combining Eqs. (4) and (17), and (23)–(25) gives

$$\gamma = 2\int \psi^{IH}(z)\,dz + \mathcal{O}(\nabla^4\rho). \tag{26}$$

Equation (26) can also be derived in a more familiar manner for a system without an external potential.[28,33] Combining Eqs. (2) and (4), and (17) gives

$$F^{tot} = 2A\int \psi^{IH}(z)\,dz - PV + \mu^{tot}N + \mathcal{O}(\nabla^4\rho). \tag{27}$$

A definition of surface tension in the absence of an external potential is

$$\gamma = \left(\frac{\partial F^{tot}}{\partial A}\right)_{T,N,V}. \tag{28}$$

Combining Eqs. (27) and (28) gives Eq. (26).

2. Obtaining homogeneous properties

It is tempting to assume that the integrands in Eqs. (23) and (26) are equal locally, allowing one to obtain $2\psi^{IH}(z)$ from $P_N(z) - P_T(z)$. This is true of the form of the pressure tensor first proposed by Lovett.[33,46,47] This form furthermore satisfies the mechanical stability restriction placed on P_N given in Eq. (18). However, no contour [such as the IK contour given in Eq. (14)] or virial-type expression was given to calculate this form of $\mathbf{P}(\mathbf{r})$ in a discrete-particle system. Simulations show that this approach does not work for the IK pressure tensor (see Fig. 4 below). This is because $P_N(z) - P_T(z)$ calculated using the IK contour and $2\psi^{IH}(z)$ differ by some function that integrates to zero over the length of the system in the z direction.

Another expression for γ was obtained by Triezenberg and Zwanzig[48] (TZ). (See also Ref. 49 for an independent derivation.) For our system,

$$\gamma = \frac{1}{2}\pi\,k_B\,T\int dz\,\rho'(z)\int dz_2\,\rho'(z_2)\int ds\,s^3\,C(z, z_2, s), \tag{29}$$

where $s = \sqrt{x_{12}^2 + y_{12}^2}$ and $C(z, z_2, s)$ is the inhomogeneous direct correlation function.

Combining Eqs. (26) and (29) without integrating over dz yields

$$\psi^{IH}(z) = \frac{1}{4}\pi\,k_B\,T\,\rho'(z)\int dz_2\,\rho'(z_2)\int ds\,s^3\,C(z, z_2, s) + \Delta_{TZ}(z) + \mathcal{O}(\nabla^4\rho), \tag{30}$$

where $\int \Delta_{TZ}(z)\,dz = 0$.

The expressions for ψ^{IH} given by Eq. (30) and the VdW method are closely related: If we approximate $C(z, z_2, s)$ as the homogeneous direct correlation function $C^0(r_{12}, \rho(z))$ and expand $\rho'(z_2)$ around $\rho'(z)$ using a Taylor series, then the resulting first term of the series is equal to Eq. (5) with $c(\rho)$ given by Eq. (6).[31,50] Furthermore, with these approximations, $\Delta_{TZ}(z) = \mathcal{O}(\nabla^4\rho)$. As a practical matter, we assume $\Delta_{TZ}(z) = 0$ in Eq. (30). Simulation results (below) confirm this as reasonable.

The use of Eq. (30) requires the inhomogeneous direct correlation function. Obtaining inhomogeneous direct correlation functions directly from simulations[51–53] and integral equation theory[54,55] has been discussed previously, but this was beyond the scope of this paper. Instead, we used the homogeneous direct correlation function at an average density to approximate the inhomogeneous direct correlation function as

$$C(z_1, z_2, s) = C^0(r_{12}, \bar{\rho}), \tag{31}$$

where $\bar{\rho} = [\rho(z_1) + \rho(z_2)]/2$. This approximation has been used previously for the LJ fluid with satisfactory results.[56]

We furthermore estimated the homogeneous direct correlation function using the homogeneous Ornstein–Zernicke (OZ) equation[57] with the Percus–Yevick (PY) closure relation.[58] A solution was effected by the method of Gillian[59] and a computer code adapted from Lee[60] with a grid spacing of $\triangle\rho^* = 0.01$ and $\triangle r^* = 0.05$ (quantities defined below). The double integral in Eq. (30) was evaluated numerically for 250 points in the z direction. The ψ^{IH} values at these points were then fit versus density using a polynomial with 15 coefficients.

Given ψ^{IH} from Eq. (30) and the approximation in Eq. (31), one can calculate ψ^0 using Eq. (17) and μ^0 using Eq. (10). In this paper, we refer to this as the *TZ method* of obtaining μ^0. If desired, one can use the TZ method to calculate P^0 using Eq. (12).

D. Long-range corrections

When simulating homogeneous systems of Lennard-Jones (LJ) particles using MD simulations, the intermolecular force is usually truncated at some radial distance r_c, and standard long-range corrections (LRCs), which assume the radial distribution function is unity for $r \geq r_c$, are applied to the energy and pressure terms at the end of the simulation.[61] Long-range forces cancel by symmetry, so there is no LRC applied to the forces for a homogeneous or isotropic system.

However, for an inhomogeneous simulation, the corrections of energy, force, and pressure tensor are nonlocal terms which depend on the condition of the surrounding fluid. Long-range forces no longer cancel, and a correction to the forces must be applied at every timestep to obtain the correct density profile. For homogeneous LJ simulations, $r_c = 2.5\sigma$ is considered reasonable, where σ is the LJ distance parameter. However, the phase behavior, including the critical point, of an inhomogeneous LJ fluid depends highly upon the cutoff distance for $r_c < 5.5\sigma$ if no long-range forces are applied.[62]

In this work, we use $r_c = 5.5\sigma$ to account for the inhomogeneity of the system. To account for interactions beyond this cutoff, the standard homogeneous LRC to pressure,[3] evaluated at $\rho(z)$, is also applied to $P^0(z)$. More accurate alternatives exist,[22] such as slab-based methods[63] or a lattice sums,[64,65] but these are more computationally expensive. We plan to investigate the effects of different LRC techniques on the CPP method and extend the CPP method to Coulombic interactions in a subsequent paper.

III. SIMULATION DETAILS

In order to test the results of the proposed methods, we selected and simulated supercritical, two-phase, vapor, and liquid conditions for a pure-component LJ fluid with ε and σ being the respective energy and distance parameters. Results in this work are given in reduced LJ units as $z^* = z/\sigma$, $T^* = k_B T/\varepsilon$, $\rho^* = \rho\sigma^3$, $\psi^* = \psi\sigma^3/\varepsilon$, $\gamma^* = \gamma\sigma^2/\varepsilon$, $\mu^* = \mu/\varepsilon$, $c^* = c/(\varepsilon\sigma^5)$, and $t^* = t/\sqrt{\sigma^2 m/\varepsilon}$.

The molecular dynamics method was used. The equations of motion included an integral-control (Nosé-Hoover) thermostat and were integrated using a 4th-order Gear predictor-corrector scheme.[61] The size of the time step was selected for each simulation to generate a root-mean-square displacement of molecules of 0.003σ per timestep. A Verlet neighbor list was used to speed up computations.[61]

The external potential was of the following form consistent with periodic boundary conditions:

$$U^{\mathrm{ext}}(z) = \frac{\triangle U_{\max}}{2} \cos\left(\frac{2\pi z}{L_z}\right), \tag{32}$$

where $\triangle U_{\max}$ is an adjustable parameter corresponding to the maximum difference in external potential. $\triangle U_{\max}$ also corresponds to maximum difference in μ^{int} as shown by Eq. (7). Changing $\triangle U_{\max}$ and the average density of the system ρ_{avg} allows one to control the range of densities obtained in a CPP simulation. In this work, we used an iterative process or an equation of state to determine $\triangle U_{\max}$ and ρ_{avg} which give a desired range of densities. Though not done here, one could use an NPT ensemble to control the average density of the system and a feedback control system for the external field to achieve a desired density profile.

The CPP method applies a continuous, spatially-varying external field to the system. This causes a continuous change in the density profile. Therefore, the CPP method essentially gives the density profile and resulting chemical potential as continuous curves. Any discretization used is for convenience in postprocessing the results. Samples for density and pressure profiles were taken every 8 timesteps and were collected using 401 equally spaced slabs normal to the z direction.

Resulting pressure and density profiles were each fit using a Fourier cosine series, as this automatically satisfies the periodicity and symmetry of the system. Additionally, limiting the number of terms in the Fourier cosine series worked well to screen out noise and smooth the data. Figure 2 shows an example of a Fourier cosine series used to fit the data. Using too few Fourier coefficients results in a poor fit of the data or oscillations near sharp changes in the profiles (such as the change in density at an interface between two phases), which biases the results. Using too many Fourier coefficients increases the random noise in the results. Using both a slab-based histogram and a Fourier fit allowed us to check the reasonableness of the fit while smoothing out random error. In order to check that our results were independent of the number of slabs used, we increased the number of slabs from 401 to 701 for the CPP 2 and 3L simulations (described below).

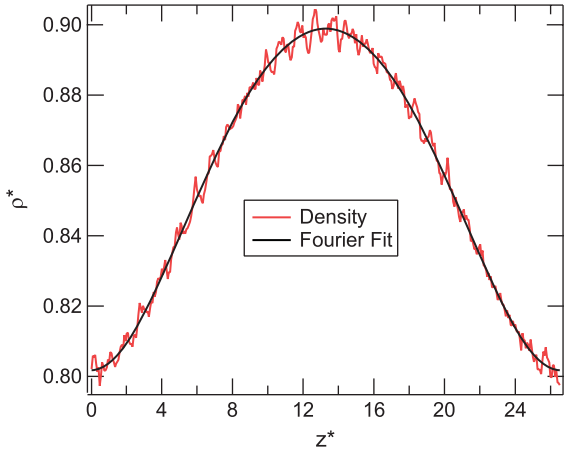

FIG. 2. An example of a Fourier fit used to smooth the density profile.

TABLE I. Parameters fopcthe CPP simulations shown in this work. Type SC refers to supercritical, 2ϕ refers to two-phase, Vap refers to vapor, and Liq refers to liquid.

Name	Type	N	$\frac{L_z}{L_x=L_y}$	T^*	$\rho^*_{\min}$	ρ^*_{avg}	$\rho^*_{\max}$	$\triangle U^*_{\max}$	timesteps
1	SC	2×10^3	2	1.5	0.043	0.437	0.749	5.0	5×10^6
1L	SC	10^4	10	1.5	0.044	0.437	0.751	5.0	10^6
2	SC	4×10^3	4	2.0	0.011	0.632	1.05	28.5	10^6
3	2ϕ	10^3	1	0.8	1.68×10^{-3}	0.403	0.847	2.0	2×10^6
3L	2ϕ	4×10^3	4	0.8	1.49×10^{-3}	0.403	0.848	2.0	2×10^6
4	Vap	10^3	1	0.8	8.35×10^{-4}	2.44×10^{-3}	4.98×10^{-3}	1.39	5×10^6
5	Liq	4×10^3	2	0.8	8.02	8.54	8.99	2.15	2×10^6

These simulations contain relatively sharp changes in density profile, and yet increasing the number of slabs did not significantly alter the $\mu^0(z)$ curves.

When assessing the results of a method, it is important to consider both random errors and systematic bias. Sources of random errors in the CPP method include noise in the measured density and pressure tensor profiles. Sources of biases in the CPP method include truncation errors in the Fourier series used to fit the profiles and truncation errors in the Taylor series expansions used to approximate μ^{IH}.

Random errors were estimated using the block method. Each simulation was divided into ten blocks, which were used to calculate 95% confidence intervals (CIs) of the data using the Student's t-distribution. In the CPP method, both the measured density and chemical potential vary at a given position. The variation in chemical potential is due to the correction for the inhomogeneity of the system. Thus a plot of μ vs ρ requires error bars in both directions. We plotted these error bars for several points along the curves in order to give the reader a sense of the random errors in the simulations.

In order to estimate the bias in the CPP method, we used an equation of state (EOS) for the LJ fluid proposed by Kolafa and Nezbeda,[66] as well as Widom's method [see Eq. (1)]. This LJ EOS and Widom's method both give the chemical potential in excess of an ideal gas. In order to obtain the full chemical potential, it is necessary to include the ideal gas chemical potential μ^{ig} given in reduced LJ units as

$$\mu^{\text{ig}*}(z) = T^* \ln\left[\left(\frac{h^{*2}}{2\pi T^*}\right)^{3/2} \rho^*(z)\right], \tag{33}$$

where $h^* = h/\sqrt{\sigma^2 \varepsilon m}$, h is Planck's constant, and m is the particle mass. For purposes of presentation, we used $h^* = 0.183$, obtained by using typical LJ parameters for argon.

The CPP method gives differences in chemical potentials as a function of density. Another method such as Widom's or an EOS is needed to determine the unknown constant (or offset) μ^{tot}. In this work, μ^{tot} was determined by shifting the $\mu^0(z)$ curve vertically until it matched the LJ EOS at ρ_{avg} (unless otherwise noted). Because μ^0 is fixed at this point, the apparent error at this point will be zero. Alternatively, we could have determined μ^{tot} by performing Widom insertions in one slice of the CPP simulation or in a separate homogeneous simulation at one density contained in the CPP simulation. It was not necessary to determine P^* because the IK method was used to calculate the pressure tensor.

IV. SIMULATION RESULTS AND DISCUSSION

Table I shows the parameters for the CPP simulations presented in this work. For reference, the critical temperature of the LJ fluid is around $T^* = 1.326$.[67] In order to allow other researchers to verify, repeat, and assess our results, we have included a spreadsheet containing a copy of the numerical data used to create our figures in the supplemental materials.[68]

A. Supercritical simulations

In the absence of an external field, a pure-component fluid at temperatures above its critical temperature will not spontaneously split into different phases. However, the addition of a spatially varying external potential produces equilibrium density gradients (and therefore surface tension as predicted by density gradient theory).

A snapshot, as well as the external potential and density profile versus position z, of CPP simulation 1 are shown above in Fig. 1. If no external field were present, this simulation would have the uniform density ρ^*_{avg} shown in Table I. We used Eq. (15) to verify the system was at mechanical equilibrium and that P_{N} was calculated accurately using Eqs. (13) and (14). Agreement between left-hand and right-hand sides of Eq. (15) was essentially exact.

Figure 3 shows the resulting homogeneous chemical potential using the three different approximations of μ^{IH}, as well as the μ^{IH} curves themselves. Results are validated by comparing to those for the LJ EOS. The curve labeled as LJ EOS in Fig. 3(b) is estimated using Eq. (9) with μ^0 given by the LJ EOS. For this system, the most accurate method of approximating μ^{IH} is the pressure tensor method, and the TZ method also works well. The VdW method is not as satisfactory, but does show the correct trend.

Figure 4 shows profiles of inhomogeneous free energy density versus position for CPP simulation 1 predicted using the VdW and TZ methods. For the VdW method, we used a value of $c^* = 4.4$ (constant with respect to density).[34] Figure 4 also shows $[P_{\text{N}}(z) - P_{\text{T}}(z)]/2$ calculated using the IK contour is not equivalent to the predicted $\psi^{\text{IH}}(z)$. Calculating the apparent (induced) surface tension using the TZ equation [Eq. (29) and the approximation given in Eq. (31)] gave $\gamma^*_{\text{TZ}} = 0.357 \pm 0.001$. Using the pressure tensor [Eq. (23)] gave $\gamma^*_{\text{IK}} = 0.311 \pm 0.015$. When an inhomogeneous long-range correction[63] was included with

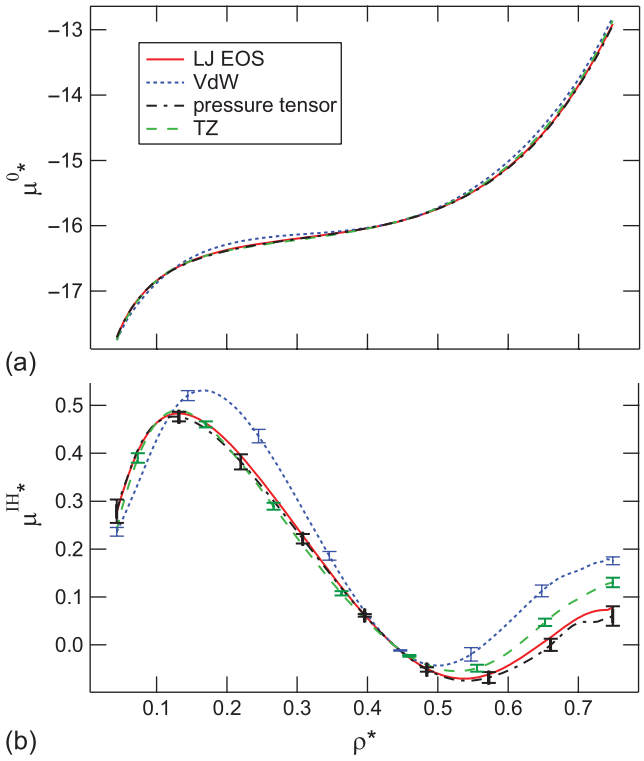

FIG. 3. (a) Homogeneous chemical potential vs density for CPP simulation 1 using three different approximations of $\mu^{\mathrm{IH}}(z)$. (b) Comparison of the different approximations of $\mu^{\mathrm{IH}}(z)$ vs density. Density error bars are not shown for the VdW and TZ curves, but are identical to those shown for the pressure tensor curve.

the pressure tensor, $\gamma^*_{\mathrm{IK}} = 0.362 \pm 0.015$, producing better agreement between the two methods and further validating the approximation given in Eq. (31). The VdW method predicted a surface tension of $\gamma^*_{\mathrm{VdW}} = 0.319 \pm 0.001$.

In order to test the influence of simulation cell length, we repeated CPP simulation 1 with length in the z direction increased by a factor of 5 (see Table I). We refer to this simulation as 1L (where L stands for *long*). Figure 5 shows that increasing L_z decreases μ^{IH} as expected from gradient theory. The CPP 1 simulation (without a correction for the inhomogeneity of the system) has much greater error than the CPP 1L simulation (also without a correction). In theory, one could increase the length of the simulation cell until μ^{IH} becomes negligible. However, Fig. 5 also shows that if an appropriate gradient correction for μ^{IH} is used, one can obtain satisfactory results using a much shorter simulation cell. Obviously, if the simulation cell is too short, the correction becomes less reliable due to large density gradients. Furthermore, the use of large external field gradients can produce anomalous layering structures in the fluid.

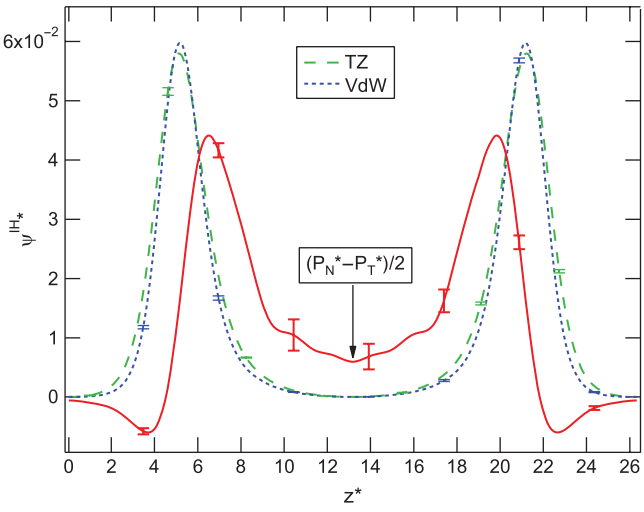

FIG. 4. Plot of inhomogeneous free energy density vs position for CPP simulation 1 predicted using the VdW and TZ methods. The quantity $[P_{\mathrm{N}}(z) - P_{\mathrm{T}}(z)]/2$ (calculated using the IK contour) is also shown, which does not match the predicted $\psi^{\mathrm{IH}}(z)$.

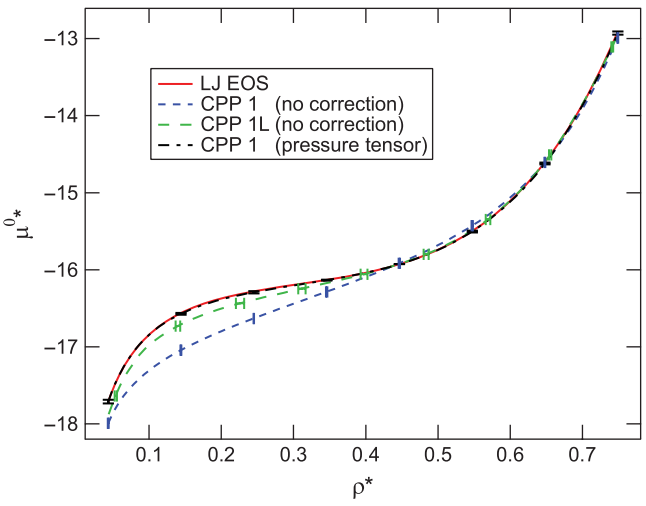

FIG. 5. Comparison of homogeneous chemical potential vs density for CPP simulations 1 and 1L. Simulation 1L is 5 times longer in the z direction than simulation 1. Density error bars for the CPP1 curve with the pressure tensor correction are not shown but are identical to those shown for the CPP1 curve without a correction.

The TZ and VdW methods take the derivative of ψ^0 to get μ^0, which may magnify noise in the data. The pressure tensor method integrates P^0 to get μ^0, which may smooth out noise in the data. Also, the pressure tensor is relatively easy to calculate. Therefore, the pressure tensor method to obtain μ^0 is the preferred method in this work and is used exclusively in the following results.

Figure 6 shows the results of supercritical CPP simulation 2 using a higher temperature and field strength than simulation 1. The highest density in this simulation was essentially at the liquid-solid coexistence point of liquid $\rho^* = 1.06$.[69] Figure 6 also shows the results of homogeneous simulations using Widom's method [Eq. (1)] for 12 discrete densities. These simulations included 10^3 particles and were run for 10^6 timesteps after equilibration. 10^3 insertions at random locations were performed every 8 timesteps. Each simulation was broken into ten blocks, which were used to calculate 95% CIs (using the Student's t-distribution) shown as error bars in Fig. 6. The simulations used $r_{\mathrm{c}} = 2.5\sigma$, and the standard LRC for chemical potential[3] was included. Relative error $\varepsilon = (\mu^0 - \mu^0_{\mathrm{LJ\,EOS}})/\Delta U^*_{\mathrm{max}}$ is also shown for the CPP and Widom's methods in Fig. 6.

The CPP method and Widom's method have different convergence properties. Widom's method converges rapidly

TABLE II. Predicted binodal and spinodal densities at $T^* = 0.8$ from CPP simulations 3 and 3L and the LJ EOS.

	Binodal ρ^*		Spinodal ρ^*	
	vapor	liquid	vapor	liquid
CPP 3	0.00413 ± 0.00019	0.805 ± 0.003	0.0512 ± 0.0027	0.673 ± 0.005
CPP 3L	0.00356 ± 0.00053	0.802 ± 0.001	0.0467 ± 0.0023	0.660 ± 0.005
LJ EOS	0.00608	0.800	0.0654	0.654

for lower densities but converges more slowly as the density of the system is increased. For this system, Widom's method starts to become biased above around $\rho^* = 0.9$, where the probability of a favorable insertion is comparatively low. The total CPU time (after equilibration) used in the 12 Widom simulations was close to that of CPP simulation 2. One could further optimize the efficiency of Widom's method by sampling less at lower densities and more at higher densities. However, the spherical LJ model represents a best-case scenario for Widom's method; Widom's method converges even more slowly for large or structured molecules. The CPP method seems to work well for low and high densities. The CPP method also gives a whole curve in a single simulation, while several simulations at different densities using Widom's method are necessary to obtain comparable results.

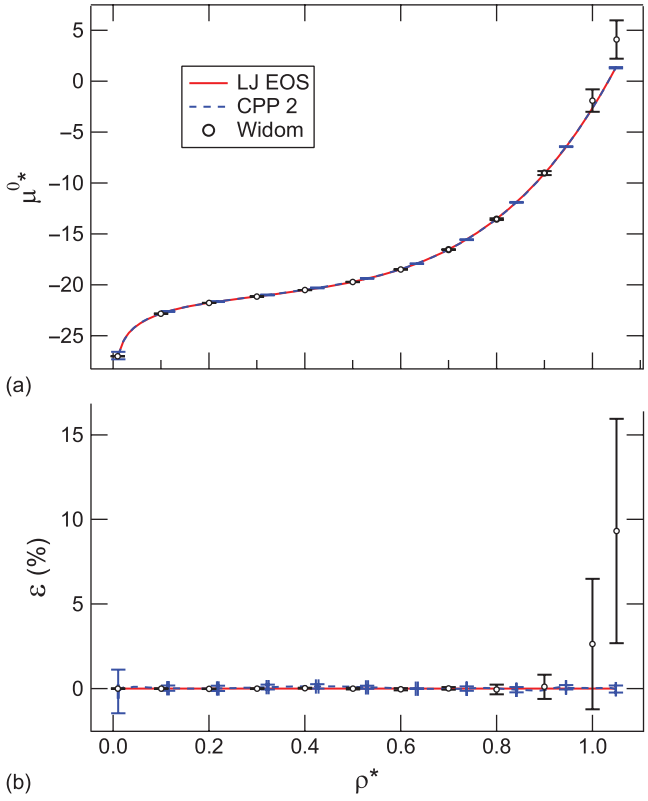

FIG. 6. (a) Homogeneous chemical potential vs density for CPP simulation 2. Results from Widom's method are also shown. (b) Relative error as compared to the LJ EOS. The error bar visible at the lowest density is for the CPP method. Density error bars for the CPP method are not shown in (a) but are identical to those shown in (b).

B. Subcritical simulations

1. Two-phase systems

In simulations below the critical temperature, the fluid can spontaneously split into two phases. The addition of an external field merely increases the inhomogeneity of a two-phase system.

Figure 7 shows results of subcritical CPP simulations 3 and 3L, which included vapor, liquid, and two-phase regions. The constant μ^{tot} was determined by fitting the μ^0 curve to the LJ EOS at one liquid density ($\rho^* = 0.83$) at which the EOS is expected to be accurate. Figure 7 also shows that μ^0 exhibits a van der Waals loop in the two-phase region. The liquid-vapor tie line calculated using the LJ EOS is shown for reference in Fig. 7. The μ^0 curves given by simulations 3 and 3L were fit using a Fourier cosine series.

Normally, two-phase molecular simulations predict coexisting densities by ignoring the interface and measuring average bulk-phase densities. In this work we determined the coexisting densities by equating the homogeneous pressures and the chemical potentials of the two phases predicted from simulation (because the external field disrupts bulk regions of constant density). The vapor–liquid coexisting (binodal) densities determined from CPP simulations 3 and 3L and the LJ EOS are shown in Table II. Liquid binodal densities show satisfactory agreement with the LJ EOS, but vapor binodal densities are not as satisfactory. Increasing the cutoff radius or using an inhomogeneous LRC may improve results.

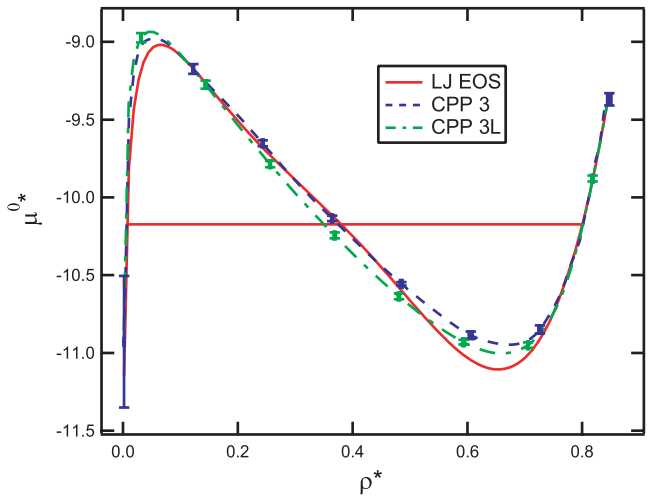

FIG. 7. Homogeneous chemical potential vs density for two-phase CPP simulations 3 and 3L. The liquid–vapor tie line calculated using the LJ EOS is shown for reference.

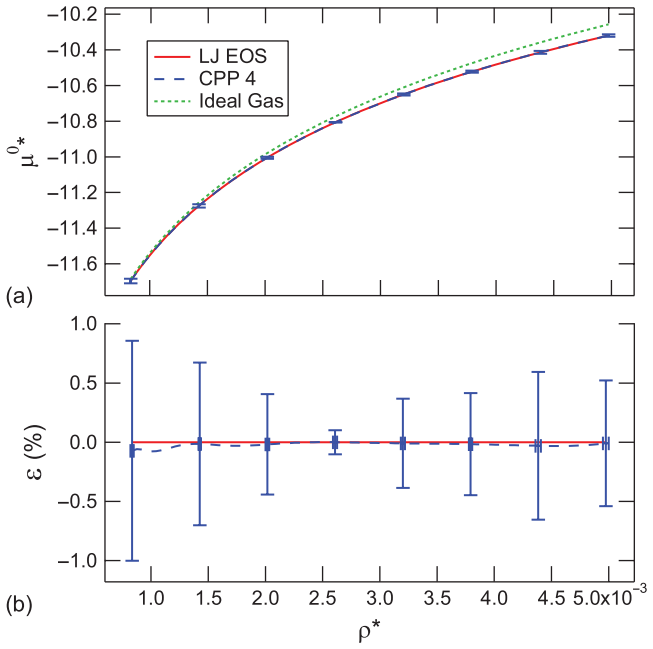

FIG. 8. (a) Homogeneous chemical potential vs density for vapor-phase CPP simulation 4, which shows slight nonideal gas behavior. (b) Relative error as compared to the LJ EOS. Density error bars for the CPP method are not shown in (a) but are identical to those shown in (b).

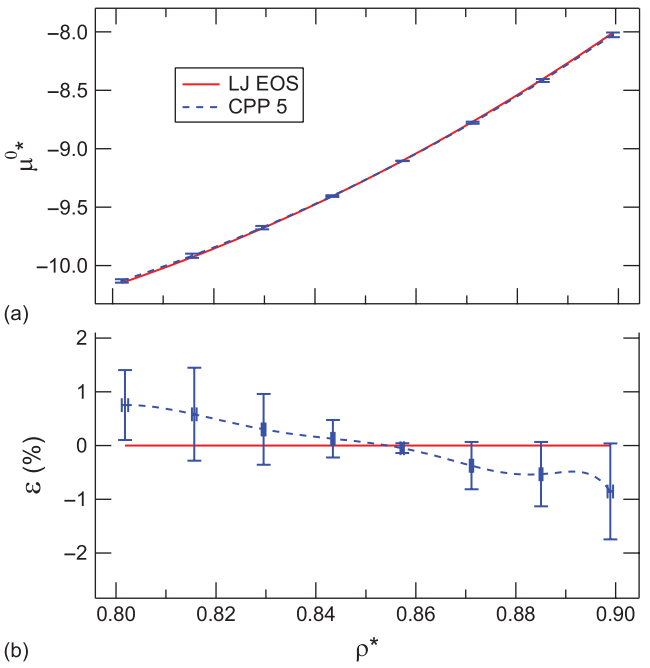

FIG. 9. (a) Homogeneous chemical potential vs density for liquid-phase CPP simulation 5. (b) Relative error as compared to the LJ EOS. Density error bars for the CPP method are not shown in (a) but are identical to those shown in (b).

The spinodal densities can be estimated by finding the minimum and maximum of the van der Waals loop in the homogeneous pressure profile predicted using Eq. (21).[70,71] We show the resulting spinodal densities from simulations 3 and 3L compared to the LJ EOS in Table II. The CPP method allows one to obtain information about the metastable or unstable regions of the system that is difficult or impossible to determine experimentally. However, a potential problem with the use of Eq. (21) in the two-phase region is that one cannot eliminate or significantly decrease the inhomogeneity in the two-phase region by increasing the length of the simulation cell. If density gradients in this region are too large, the pressure tensor correction for the inhomogeneity of the system could be less reliable. We also note that it is difficult to validate spinodal densities using the LJ EOS because the EOS was not fit with data in the metastable or unstable regions. Vapor binodal and spinodal densities were also somewhat sensitive to the number of Fourier cosine terms used to fit the profiles.

Figure 7 also shows that for this simulation setup, random errors in the CPP method become significant at very low densities. This problem is easily overcome by performing a separate CPP simulation exclusively at vapor conditions as described below.

2. Single-phase systems

If one is interested only in the vapor or liquid regions (a single phase) of a subcritical fluid, a CPP simulation can be performed only at these conditions. The effect of an external potential on a single-phase subcritical fluid is similar to that for the supercritical case. Figure 8 shows the results of vapor-phase CPP simulation 4. The results show slight departure from ideal gas behavior and also show that the CPP method works well at predicting the chemical potential at low densities. The agreement between CPP and the LJ EOS is better than the size error bars would suggest. For this simulation, there appears to be cancellation of errors when the pressure tensor correction is used. This may be because errors in the fits of the density and pressure tensor are correlated in this instance.

Figure 9 shows the results of liquid-phase CPP simulation 5. At this temperature, the density at the liquid-solid coexistence point is liquid $\rho^* = 0.881$,[69] so part of the results represent a metastable liquid region. These results show the CPP method also works well to determine chemical potential differences at liquid densities. There also appears to be a slight systematic disagreement between the results for this CPP simulation and the Kolafa and Nezbeda EOS.

V. CONCLUSION

A new method, called chemical potential perturbation (CPP), has been developed to predict the chemical potential in periodic molecular simulations. The CPP method applies a spatially varying external potential to the simulation, causing the density to depend upon position in the simulation cell. Following equilibration the homogeneous (uniform or bulk) chemical potential as a function of density can be determined relative to some reference state after correcting for the effects of the inhomogeneity of the system. If desired, the homogeneous pressure and Helmholtz free energy can also be predicted by the new method, as well as binodal and spinodal densities of a two-phase fluid.

We compare three different methods of approximating the inhomogeneous correction. The VdW method uses the van der Waals density gradient theory to approximate the

inhomogeneous Helmholtz free energy density. The pressure tensor method uses the local pressure tensor to approximate the homogeneous pressure. The TZ method uses the Triezenberg–Zwanzig definition of surface tension to approximate the inhomogeneous free energy density. The pressure tensor and TZ methods give satisfactory results, while results from the VdW method show the correct trend. Increasing the simulation cell length may decrease the inhomogeneity of the system, but the use of a correction allows one to obtain satisfactory results using a much shorter simulation cell or work with natural two-phase systems. Due to the ease of calculation, the pressure tensor method is the preferred method for obtaining homogeneous properties in this work.

The CPP method was tested using a pure-component LJ fluid at vapor, liquid, two-phase, and supercritical conditions. Satisfactory agreement was found between the CPP method and an LJ equation of state. The efficiency of the CPP method was also compared to that for Widom's method under the tested conditions. Both Widom's method and the CPP method work well for low densities, and the CPP method also works well for high densities where Widom's method starts to fail.

We have used a relatively simple form for the external potential in this work. More complicated forms could be used to further decrease the density gradients in the simulation. In a subsequent paper, we plan to discuss different long-range corrections to the pressure tensor. It is straightforward to extend the CPP method to structured molecules and we expect that the method will still work well, even for high densities. Particle insertions would only be necessary to determine the constant μ^{tot} if an ideal gas reference state is not contained in the CPP simulation, and such insertions can be performed at the lowest density in the simulation. We also plan to extend the CPP method to multicomponent systems.

ACKNOWLEDGMENTS

This work was supported by the National Science Foundation (NSF), CTS 0547610. We thank Professor Richard Rowley for providing helpful discussions and resources related to this work.

[1] G. Job and F. Herrmann, Eur. J. Phys. **27**, 353 (2006).
[2] R. Baierlein, Am. J. Phys. **69**, 423 (2001).
[3] D. Frenkel and B. Smit, *Understanding molecular simulation: from algorithms to applications* (Academic, San Diego, 2002).
[4] K. E. Gubbins, Mol. Simul. **2**, 223 (1989).
[5] B. Widom, J. Chem. Phys. **39**, 2808 (1963).
[6] B. Widom, J. Phys. Chem. **86**, 869 (1982).
[7] B. Widom, J. Stat. Phys. **19**, 563 (1978).
[8] C. H. Bennett, J. Comput. Phys. **22**, 245 (1976).
[9] G. L. Deitrick, L. E. Scriven, and H. T. Davis, J. Chem. Phys. **90**, 2370 (1989).
[10] P. Jedlovszky and M. Mezei, J. Am. Chem. Soc. **122**, 5125 (2000).
[11] R. Delgado-Buscalioni, G. De Fabritiis, and P. V. Coveney, J. Chem. Phys. **123**, 9 (2005).
[12] G. C. Boulougouris, Mol. Phys. **96**, 905 (1999).
[13] K. Ding and J. P. Valleau, J. Chem. Phys. **98**, 3306 (1993).
[14] K. K. Mon and R. B. Griffiths, Phys. Rev. A **31**, 956 (1985).
[15] K. S. Shing and K. E. Gubbins, Mol. Phys. **43**, 717 (1981).
[16] J. Kolafa and I. Nezbeda, Mol. Simul. **5**, 391 (1991).
[17] P. Attard, J. Chem. Phys. **98**, 2225 (1993).
[18] K. S. Shing and K. E. Gubbins, Mol. Phys. **46**, 1109 (1982).
[19] D. A. Kofke and P. T. Cummings, Mol. Phys. **92**, 973 (1997).
[20] A. Z. Panagiotopoulos, Mol. Phys. **61**, 813 (1987).
[21] A. Z. Panagiotopoulos, N. Quirke, M. Stapleton, and D. J. Tildesley, Mol. Phys. **63**, 527 (1988).
[22] J. Wang and X. C. Zeng, J. Theor. Comput. Chem. **8**, 733 (2009).
[23] M. Rao and D. Levesque, J. Chem. Phys. **65**, 3233 (1976).
[24] R. L. Rowley, T. D. Shupe, and M. W. Schuck, Mol. Phys. **82**, 841 (1994).
[25] M. Henrichsen and R. L. Rowley, Fluid Phase Equilib. **137**, 75 (1997).
[26] J. G. Powles, B. Holtz, and W. A.B. Evans, J. Chem. Phys. **101**, 7804 (1994).
[27] W. Humphrey, A. Dalke, and K. Schulten, J. Mol. Graphics **14**, 33 (1996).
[28] H. T. Davis, *Statistical mechanics of phases, interfaces, and thin films* (VCH, New York, 1996).
[29] J. D. van der Waals, Z. Phys. Chem., Stoechiom. Verwandtschaftsl. **13**, 657 (1894).
[30] J. S. Rowlinson, J. Stat. Phys. **20**, 197 (1979).
[31] J. S. Rowlinson and B. Widom, *Molecular theory of capillarity* (Clarendon, Oxford, 1982).
[32] J. W. Cahn and J. E. Hilliard, J. Chem. Phys. **28**, 258 (1958).
[33] A. J.M. Yang, P. D. Fleming, and J. H. Gibbs, J. Chem. Phys. **64**, 3732 (1976).
[34] D. Duque, J. C. Pamies, and L. F. Vega, J. Chem. Phys. **121**, 11395 (2004).
[35] J. H. Irving and J. G. Kirkwood, J. Chem. Phys. **18**, 817 (1950).
[36] P. Schofield and J. R. Henderson, Proc. R. Soc. London, Ser. A **379**, 231 (1982).
[37] A. Harasima, Adv. Chem. Phys. **1**, 203 (1958).
[38] J. G. Kirkwood and F. P. Buff, J. Chem. Phys. **17**, 338 (1949).
[39] J. P. R. B. Walton, D. J. Tildesley, J. S. Rowlinson, and J. R. Henderson, Mol. Phys. **48**, 1357 (1983).
[40] J. P. R. B. Walton, Mol. Phys. **58**, 1013 (1986).
[41] F. Goujon, P. Malfreyt, J. M. Simon, A. Boutin, B. Rousseau, and A. H. Fuchs, J. Chem. Phys. **121**, 12559 (2004).
[42] B. S. Carey, L. E. Scriven, and H. T. Davis, J. Chem. Phys. **69**, 5040 (1978).
[43] H. T. Davis and L. E. Scriven, Adv. Chem. Phys. **49**, 357 (1982).
[44] S. M. Oversteegen, P. A. Barneveld, F. A.M. Leermakers, and J. Lyklema, Langmuir **15**, 8609 (1999).
[45] F. P. Buff, J. Chem. Phys. **23**, 419 (1955).
[46] D. Lamoen and N. H. March, Phys. Chem. Liq. **38**, 495 (2000).
[47] R. A. Lovett, Ph.D. dissertation, University of Rochester, 1965.
[48] D. G. Triezenberg and R. Zwanzig, Phys. Rev. Lett. **28**, 1183 (1972).
[49] R. Lovett, P. W. DeHaven, J. James, J. Vieceli, and F. P. Buff, J. Chem. Phys. **58**, 1880 (1973).
[50] J. R. Henderson, Mol. Phys. **39**, 709 (1980).
[51] J. Stecki and S. Toxvaerd, J. Chem. Phys. **103**, 9763 (1995).
[52] J. Stecki, J. Chem. Phys. **109**, 5002 (1998).
[53] J. Stecki and S. Toxvaerd, J. Chem. Phys. **117**, 2860 (2002).
[54] I. Omelyan, A. Kovalenko, and F. Hirata, Chem. Phys. Lett. **397**, 368 (2004).
[55] I. Omelyan, F. Hirata, and A. Kovalenko, Phys. Chem. Chem. Phys. **7**, 4132 (2005).
[56] C. Ebner, W. F. Saam, and D. Stroud, Phys. Rev. A **14**, 2264 (1976).
[57] L. S. Ornstein and F. Zernike, Proc. R. Acad. Sci. Amsterdam **17**, 793 (1914).
[58] J. K. Percus and G. J. Yevick, Phys. Rev. **110**, 1 (1958).
[59] M. J. Gillan, Mol. Phys. **38**, 1781 (1979).
[60] L. L. Lee, *Molecular thermodynamics of nonideal fluids* (Butterworths, Boston, 1988).
[61] M. Allen and D. Tildesley, *Computer simulation of liquids* (Oxford Science, 1989).
[62] A. Trokhymchuk and J. Alejandre, J. Chem. Phys. **111**, 8510 (1999).
[63] J. Janecek, J. Phys. Chem. B **110**, 6264 (2006).
[64] N. Karasawa and W. A. Goddard, J. Chem. Phys. **93**, 7320 (1989).
[65] J. Lopez-Lemus and J. Alejandre, Mol. Phys. **100**, 2983 (2002).
[66] J. Kolafa and I. Nezbeda, Fluid Phase Equilib. **100**, 1 (1994).
[67] J. M. Caillol, J. Chem. Phys. **109**, 4885 (1998).
[68] See supplementary material at http://dx.doi.org/10.1063/1.3561865 for a spreadsheet containing the numerical data used to create the figures appearing in this paper.
[69] M. A. van der Hoef, J. Chem. Phys. **113**, 8142 (2000).
[70] A. R. Imre, G. Mayer, G. Hazi, R. Rozas, and T. Kraska, J. Chem. Phys. **128**, 114708 (2008).
[71] T. Kraska, F. Romer, and A. R. Imre, J. Phys. Chem. B **113**, 4688 (2009).